arXiv:hep-ex/0208042v1 26 Aug 2002

EUROPEAN ORGANIZATION FOR NUCLEAR RESEARCH

CERN-EP/2002-066
August 2, 2002

Search for Neutral Higgs Bosons of the Minimal Supersymmetric Standard Model in e^+e^- Interactions at $\sqrt{s}$ up to 209 GeV

L3 Collaboration

Abstract

A search for the lightest neutral CP-even and neutral CP-odd Higgs bosons of the Minimal Supersymmetric Standard Model is performed using 216.6 pb^{-1} of data collected with the L3 detector at LEP at centre-of-mass energies between 203 and 209 GeV. No indication of a signal is found. Including our results from lower centre-of-mass energies, lower limits on the Higgs boson masses are set as a function of $\tan\beta$ for several scenarios. For $\tan\beta$ greater than 0.7 they are $m_{\mathrm{h}} > 84.5$ GeV and $m_{\mathrm{A}} > 86.3$ GeV at 95% confidence level.

Submitted to *Phys. Lett. B*

1 Introduction

In the Minimal Supersymmetric Standard Model (MSSM) [1] two doublets of complex scalar fields are required to generate the masses of gauge bosons and fermions. The neutral Higgs sector of the MSSM comprises three physical states: two CP-even Higgs bosons, the lighter of which is denoted as h and the heavier as H, and a neutral CP-odd boson, A.

The two most important production mechanisms of the light neutral Higgs boson in e^+e^- collisions are:

$$e^+e^- \to hZ, \tag{1}$$

$$e^+e^- \to hA, \tag{2}$$

with tree level cross sections that are related to the Standard Model Higgs-strahlung cross section, σ_{HZ}^{SM}, as [2]:

$$\sigma_{hZ} = \sin^2(\beta-\alpha)\sigma_{HZ}^{SM}, \tag{3}$$

$$\sigma_{hA} = \cos^2(\beta-\alpha)\tilde{\lambda}\sigma_{HZ}^{SM}, \tag{4}$$

where $\tan\beta$ is the ratio of the vacuum expectation values of the two Higgs doublets, α is the mixing angle in the CP-even Higgs boson sector and $\tilde{\lambda}$ is the p-wave suppression factor depending on the Higgs boson masses, m_h and m_A, and the centre-of-mass energy $\sqrt{s}$. For some choices of the MSSM parameters, the H boson can also be produced via the Higgs-strahlung process

$$e^+e^- \to HZ, \tag{5}$$

with a cross section suppressed by the factor $\cos^2(\beta-\alpha)$ relative to σ_{HZ}^{SM}.

For most of the MSSM parameter space considered, the neutral Higgs bosons are predicted to decay dominantly into $b\bar{b}$ and $\tau^+\tau^-$. However, in certain parameter regions, other decays like $h \to AA$ and $A \to c\bar{c}$ become important.

The search for the neutral Higgs bosons is performed in the framework of the constrained MSSM with seven free parameters. These are the universal sfermion mass parameter, M_{SUSY}, the common Higgs-squark trilinear coupling, $\mathcal{A}$, the supersymmetric Higgs mass parameter, μ, the SU(2) gaugino mass parameter, M_2, the gluino mass parameter, M_3, m_A and $\tan\beta$. The mass of the top quark is taken to be 174.3 GeV [3].

Previous searches for the neutral Higgs bosons were reported by L3 [4,5] and other experiments [6]. In this Letter, we present the results of the search for the h and A bosons using data collected with the L3 detector [7] in the year 2000. In comparison to previous analyses [4] the performance in the four-jet channel is improved by using a new likelihood based analysis. In addition, the six-jet final state resulting from the $hZ \to AAq\bar{q}$ topology is investigated.

2 Benchmark Scenarios

Due to the large number of parameters remaining in the constrained MSSM, we focus on three specific parameter settings as suggested in Reference 8. These benchmark settings are

denoted as the "$m_{\rm h}-$max", "no mixing" and "large$-\mu$" scenarios, with the corresponding MSSM parameter values detailed in Table 1. The first two scenarios take into account radiative corrections to $m_{\rm h}$ computed within a two-loop diagrammatic approach [9] and differ only by the value of $\rm X_t \equiv \mathcal{A} - \mu \cot\beta$, which governs the mixing in the scalar top sector. The "$m_{\rm h}-$max" scenario is designed to extend the search to the maximal theoretical bound on $m_{\rm h}$ for any value of tanβ and leads to rather conservative constraints on tanβ. The "no mixing" scenario corresponds to vanishing mixing in the scalar top sector and is more favorable to LEP searches. After fixing the parameters $\rm M_{SUSY}$, $\rm M_2$, μ, $\rm X_t$ and $\rm M_3$, a scan over the remaining parameters tanβ and $m_{\rm A}$ is performed in the range $0.4 \leq \tan\beta \leq 30$ and 10 GeV $\leq m_{\rm A} \leq$ 1 TeV. The widths of the h and A bosons are assumed to be smaller than the experimental mass resolutions. As this holds in these two scenarios only for $\tan\beta \leq 30$, higher values of tanβ are not considered.

In the "large$-\mu$" scenario the upper theoretical bound on $m_{\rm h}$ is slightly less than 108 GeV, thus in the LEP reach. However, for some choices of tanβ and $m_{\rm A}$, the Higgs boson pair production (2) is kinematically inaccessible and the Higgs-strahlung process (1) is strongly suppressed due to small values of $\sin^2(\beta-\alpha)$. Sensitivity in these regions can be recovered by exploiting the H boson production via the high cross section Higgs-strahlung process (5). The scan is performed over $m_{\rm A}$ from 10 GeV to 400 GeV and over tanβ between 0.7 and 50. Within this scenario, the assumption that the widths of the Higgs bosons are small compared to experimental mass resolutions is valid for tanβ up to 50. For the interpretation of the data within this "large$-\mu$" scenario, the improved one-loop renormalisation group calculations [10] are used.

3 Data and Monte Carlo Samples

The data recorded at centre-of-mass energies between 203 and 209 GeV are grouped into three data sets with effective centre-of-mass energies of 204.3, 206.1 and 208.0 GeV, corresponding to integrated luminosities of 26.0, 181.9 and 8.7 pb^{-1}. The results obtained from this data are combined with the results from integrated luminosities of 233.2 pb^{-1} at 192 GeV $< \sqrt{\rm s} <$ 202 GeV [4] and 176.4 pb^{-1} at $\sqrt{\rm s} = 189$ GeV [5].

The cross sections of processes (1), (2) and (5) and the decay branching fractions of h, H and A are calculated using the HZHA generator [11]. For efficiency studies, Monte Carlo samples of 2000 Higgs events are generated for each mass hypothesis in each search channel using PYTHIA [12] and HZHA. For the hA samples, $m_{\rm h}$ and $m_{\rm A}$ range from 50 to 105 GeV in steps of 5 GeV. For the hZ samples, $m_{\rm h}$ is chosen in steps of 5 GeV from 60 to 100 GeV and in steps of 1 GeV from 100 to 120 GeV. For background studies, the following Monte Carlo programs are used: KK2f [13] ($\rm e^+e^- \to q\bar{q}(\gamma)$), PYTHIA ($\rm e^+e^- \to ZZ$ and $\rm e^+e^- \to Ze^+e^-$), KORALW [14] ($\rm e^+e^- \to W^+W^-$) and KORALZ [15] ($\rm e^+e^- \to \tau^+\tau^-$). Hadron production in two-photon interactions is simulated with PYTHIA and PHOJET [16]. EXCALIBUR [17] is used for other four fermion final states. The number of simulated events for the most important background channels is more than 100 times the number of expected events.

The L3 detector response is simulated using the GEANT program [18], which models the effects of energy loss, multiple scattering and showering in the detector. The GHEISHA program [19] is used to simulate hadronic interactions in the detector. Time dependent detector inefficiencies, monitored during data taking, are also taken into account.

4 Analysis Procedures

For the hA production, the decay modes considered are: $hA \to b\bar{b}b\bar{b}$, $hA \to b\bar{b}\tau^+\tau^-$ and $hA \to \tau^+\tau^- b\bar{b}$. For the hZ or HZ production, the event topologies considered are: $q\bar{q}q'\bar{q}'$, $q\bar{q}\nu\bar{\nu}$, $q\bar{q}\ell^+\ell^-(\ell = e, \mu, \tau)$ and $\tau^+\tau^- q\bar{q}$. To cover the MSSM parameter regions where the decay $h \to AA$ becomes important, the $hZ \to AAq\bar{q} \to q\bar{q}q'\bar{q}'q''\bar{q}''$ channel is studied as well. Searches in channels with decays of the h boson into quarks are optimised for the dominant $h \to b\bar{b}$ decay channel. The analyses of the $q\bar{q}\nu\bar{\nu}$ and $q\bar{q}\ell^+\ell^-(\ell = e, \mu)$ final states are the same as those used in the Standard Model Higgs search [20].

4.1 The $hZ \to b\bar{b}q\bar{q}$ and $hA \to b\bar{b}b\bar{b}$ Analyses

The signature of the $hZ \to b\bar{b}q\bar{q}$ final state is four high-multiplicity hadronic jets and the presence of b hadrons, in particular in the jets expected to stem from the Higgs boson. The invariant mass of the jets supposed to originate from the Z boson must be compatible, within mass resolution, with its mass, m_Z. The $hA \to b\bar{b}b\bar{b}$ search topology is characterised by four high multiplicity hadronic jets originating from b-quarks. The main backgrounds arise from $q\bar{q}(\gamma)$ final states and hadronic decays of W-pairs and Z-pairs.

Initially, a common preselection for both the $hZ \to b\bar{b}q\bar{q}$ and $hA \to b\bar{b}b\bar{b}$ channels is applied, followed by a kinematic classification of events into hZ or hA analysis branches. Selection criteria optimised for each branch are used and a final discriminant specific to each branch is constructed.

The preselection criteria used are described in Reference 20. Events passing the preselection are forced into a four-jet topology using the Durham algorithm [21] and a kinematic fit imposing energy and momentum conservation (4C fit) is performed. Each event is tested for its compatibility with the hZ and hA production hypotheses, exploiting dijet invariant masses. There are three possibilities for pairing jets in a four-jet event. For each pairing, χ^2 values are calculated for the hypotheses of hZ and hA production:

$$\chi^2_{hZ} = \frac{(\Sigma_i - m_h - m_Z)^2}{\sigma^2_\Sigma} + \frac{(\Delta_i - |m_h - m_Z|)^2}{\sigma^2_\Delta}, \tag{6}$$

$$\chi^2_{hA} = \frac{(\Sigma_i - m_h - m_A)^2}{\sigma^2_\Sigma} + \frac{(\Delta_i - |m_h - m_A|)^2}{\sigma^2_\Delta}. \tag{7}$$

In these expressions Σ_i and Δ_i are the dijet mass sum and dijet mass difference of the i-th pairing, and σ_Σ and σ_Δ are the dijet mass sum and dijet mass difference resolution functions. They are found to be almost independent of the dijet masses for production well above threshold and are estimated from Monte Carlo to be $\sigma_\Sigma = 4$ GeV and $\sigma_\Delta = 18$ GeV. Close to the kinematic threshold they strongly depend on the dijet mass sum. For each hypothesis, the jet pairing with the smallest χ^2 is chosen and the probability $P(\chi^2)$ is calculated.

Events are assigned either to the hZ or hA analysis branch by means of a binned likelihood [20], $L^c_{hZ} \equiv 1 - L^c_{hA}$, constructed from the following variables: the χ^2 probabilities, $P(\chi^2_{hZ})$ and $P(\chi^2_{hA})$, the Higgs boson production angle, $|\cos\Theta|$, the number of charged tracks, N_{trk}, the global event b-tag, B_{tag}, and the maximum triple jet boost, γ_{triple} [20]. Events are assigned to the hZ branch if $L^c_{hZ} > 0.5$, or to the hA branch otherwise.

The selection in both branches proceeds in the same way. Events are rejected if $P(\chi^2) < 1\%$. High b-tag events are accepted and a selection likelihood is then constructed to separate the

signal from the $q\bar{q}(\gamma)$ final states and hadronic decays of W-pairs and Z-pairs, using N_{trk}, B_{tag}, γ_{triple}, $|\cos\Theta|$ and $\log Y_{34}$, where Y_{34} is the jet resolution parameter for which the event topology changes from three to four jets. A final discriminant is constructed for events passing an optimised selection likelihood cut. The optimisation is based on the analysis performance at (m_A,m_h) values close to the expected sensitivity of the L3 combined search. The final discriminants are built from individual b-tag variables of the four jets and $P(\chi^2)$. In the hZ branch, an event category variable is also used. This variable is constructed from rankings of b-tag variables of the two jets assigned to the Higgs boson, as described in Reference 20. The final discriminant in the hA branch also includes the corresponding selection likelihood.

Table 2 reports the number of data, expected background and expected signal events selected at different stages of the analysis for two representative Higgs boson mass hypotheses in the "m_h−max" scenario, (m_A,m_h) = (90,90) GeV at tanβ = 25 and (m_A,m_h) = (165,110) GeV at tanβ = 3. For these hypotheses the distribution of the final discriminant in terms of a signal-to-background ratio is presented in Figure 1. The data are compatible with the background expectation.

4.2 The hZ → $b\bar{b}\tau^+\tau^-$, $\tau^+\tau^-q\bar{q}$ and hA → $b\bar{b}\tau^+\tau^-$ Analyses

The signatures of hZ → $b\bar{b}\tau^+\tau^-$, $\tau^+\tau^-q\bar{q}$ and hA → $b\bar{b}\tau^+\tau^-$ [1)] final states are a pair of taus accompanied by two hadronic jets. For each of the channels hA and hZ an analysis is optimised based either on the tau identification or on the event topology by requiring four jets with two of them being narrow and of low multiplicity. The main background comes from W-pair decays containing taus. The analysis is similar to the one used in previous searches [4]. The selection is optimised for lower Higgs boson masses by applying looser cuts on the opening angles of the jets and tau pairs compared to the Standard Model Higgs search [20]. The invariant mass of the tau pair, $m_{\tau^+\tau^-}$, and of the hadronic jets, $m_{q\bar{q}}$, must be between 25 GeV and 125 GeV. The ratio between the total energy deposited in the detector, E_{vis}, and $\sqrt{s}$ must be less than 0.9 and the polar angle of the missing momentum, Θ_{miss}, must satisfy $|\cos\Theta_{miss}| < 0.9$.

Four possible final states are considered: hZ → $b\bar{b}\tau^+\tau^-$, hZ → $\tau^+\tau^-q\bar{q}$, hA → $b\bar{b}\tau^+\tau^-$ and hA → $\tau^+\tau^-b\bar{b}$. Each event is uniquely assigned to one channel using mass and b-tag information, and final discriminants specific to each channel are constructed. For the hZ → $b\bar{b}\tau^+\tau^-$, hA → $b\bar{b}\tau^+\tau^-$ and hA → $\tau^+\tau^-b\bar{b}$ final states, the final discriminant is constructed from $m_{q\bar{q}}$, $m_{\tau^+\tau^-}$ and the b-tag variables of the two hadronic jets. For the hZ → $\tau^+\tau^-q\bar{q}$ final state, $m_{\tau^+\tau^-}$ is used as the final discriminant.

Table 3 reports the number of data, expected background and expected signal events for the same Higgs boson masses chosen in the previous section. For these hypotheses the distribution of the final discriminant in terms of the signal-to-background ratio is shown in Figure 2. Good agreement between the data and the expected background is found.

4.3 The hZ → AA$q\bar{q}$ Channel

To improve the search sensitivity in the region of low tanβ and low m_A where the h → AA decay becomes dominant and the A → $c\bar{c}$ decay replaces A → $b\bar{b}$, a dedicated analysis is devised and performed on the data collected at $\sqrt{s}$ = 189 − 209 GeV. This analysis aims to select hZ → AA$q\bar{q}$ → $q\bar{q}q'\bar{q}'q''\bar{q}''$ final states and is derived from the analysis used in the four-jet channel. At the first stage, the same preselection as in the four-jet channel is applied with

[1)] Both of the decay modes (h→ $b\bar{b}$, A→ $\tau^+\tau^-$) and (h→ $\tau^+\tau^-$, A→ $b\bar{b}$) are considered.

an additional cut on the event thrust, $T < 0.9$. In the next step, a signal likelihood L_{AAqq} is built to distinguish the $hZ \to AAq\bar{q}$ signal from the $q\bar{q}(\gamma)$ final states and hadronic decays of W-pairs and Z-pairs. This likelihood is constructed from the variables: N_{trk}, γ_{triple}, $\log Y_{34}$, the event sphericity, the absolute value of the cosine of the polar production angle, assuming the production of a pair of gauge bosons [20] and $\log Y_{56}$, where Y_{56} is the jet resolution parameter for which the event topology changes from five to six jets. Among these variables N_{trk} and $\log Y_{56}$ have the most discriminating power between the $hZ \to AAq\bar{q}$ signal and four-fermion and two-fermion backgrounds. The likelihood L_{AAqq} is used as the final discriminant. No evidence for the $hZ \to AAq\bar{q}$ signal is found in data. As an example, Figure 3 shows the distributions of $\log Y_{56}$ and $L_{AAq\bar{q}}$ for data, the expected background and the signal corresponding to the Higgs boson mass hypothesis $(m_A, m_h) = (30, 70)$ GeV.

5 Results

The analyses presented in this Letter are combined with the $hZ \to b\bar{b}\nu\bar{\nu}$ and $hZ \to b\bar{b}\ell^+\ell^-$ ($\ell = e, \mu$) analyses used in the Standard Model Higgs searches [20]. The results of previous searches [4, 5] at lower $\sqrt{s}$ are also included. The final discriminant distributions obtained in each search channel at each centre-of-mass energy are used to evaluate the presence of a signal in the data. No evidence for a signal is found and the search results are interpreted in terms of an exclusion of MSSM parameter regions. The statistical procedure adopted for the interpretation of the data and the definition of the confidence level CL_s are described in Reference 22. The analysis performance is quantified with the expected median confidence level, CL_{med}, which is obtained from CL_s by replacing the observed value of the test-statistic $-2\ln Q$ by its background median value.

Systematic and statistical uncertainties on the signal and on the background are incorporated in the confidence level calculations as described in Reference 23. The main sources of systematic uncertainties are the detector resolution, the selection procedure, theoretical uncertainties and Monte Carlo statistics. The overall systematic uncertainty is estimated to range from 3% to 6% on the expected signal, and from 7% to 15% on the background, depending on the search channel.

5.1 Limits in the "m_h−max" and "No mixing" Scenarios

Figure 4 shows the area of the $(\tan\beta, m_h)$ and $(\tan\beta, m_A)$ planes excluded at 95% confidence level for the "m_h−max" and "no mixing" scenarios. In the "m_h−max" scenario, lower limits on the masses of the h and A bosons are set at 95% confidence level as:

$$m_A > 86.5 \text{ GeV}, \qquad m_h > 86.0 \text{ GeV},$$

for every $\tan\beta$ value considered. The expected values in the absence of a signal are $m_A > 88.6$ GeV and $m_h > 88.4$ GeV. For $0.55 < \tan\beta < 2.2$ the A boson is excluded up to a mass of 1 TeV thus allowing to rule out this $\tan\beta$ range.

In the "no mixing" scenario, the combined results establish lower mass bounds at 95% confidence level of:

$$m_A > 86.3 \text{ GeV}, \qquad m_h > 85.5 \text{ GeV}.$$

The expected limits are $m_A > 88.6$ GeV and $m_h > 88.5$ GeV. Here the $\tan\beta$ range between 0.4 and 5.4 is excluded at 95% confidence level, also for m_A up to 1 TeV. A downward fluctuation

of about 1σ compared to the background expectation is observed in the data at ($m_{\rm A}$,$m_{\rm h}$) $\sim$ (90,90) GeV. There is a deficit of candidates in the hA $\rightarrow$ b$\bar{\rm b}$b$\bar{\rm b}$ channel at $\sqrt{\rm s} = 203-209$ GeV resulting in an observation of a $\rm CL_s$ value smaller than 5% although no exclusion of this region at 95% confidence level is expected. This effect explains the irregularity in the exclusion plots at high tanβ and $m_{\rm h}$ between 86 GeV and 91 GeV. An excess in the hZ $\rightarrow$ b$\bar{\rm b}\ell^+\ell^-(\ell = {\rm e},\mu)$ channel at $m_{\rm h} \sim 90$ GeV and in the hZ $\rightarrow$ b$\bar{\rm b}$q$\bar{\rm q}$ channel in the $m_{\rm h}$ range between 90 GeV and 95 GeV, from the $\sqrt{\rm s} = 192-202$ GeV data, result in a sizable reduction of the excluded range of tanβ for the mass range 90 GeV $\lesssim m_{\rm h} \lesssim$ 100 GeV in both scenarios. The area at tan$\beta < 0.8$ and $m_{\rm A} < 40$ GeV which previously was not excluded in the "no mixing" scenario [4] is now excluded using the results of the hZ $\rightarrow$ AAq$\bar{\rm q}$ analysis[2)].

5.2 Limits in the "Large$-\mu$" Scenario

In the "large$-\mu$" scenario there are regions of the (tanβ,$m_{\rm A}$) plane where the hA process is inaccessible and the hZ process is suppressed by a small value of $\sin^2(\beta-\alpha)$. However, the heavy CP even Higgs boson H is expected to be produced there via the Higgs-strahlung process. Hence, the loss of the sensitivity for the h boson can be compensated by reinterpreting the hZ analyses in the context of the HZ search. This is illustrated in Figure 5a which presents the $(1-{\rm CL_{med}})$ confidence level calculated as a function of $m_{\rm A}$ at tan$\beta = 15$ in the context of the searches for the h and H bosons. Searches for the h boson alone lack sensitivity in the $m_{\rm A}$ range 89 GeV $\lesssim m_{\rm A} \lesssim$ 108 GeV. The inclusion of the HZ search results extends the region of sensitivity leaving only the range 89 GeV $\lesssim m_{\rm A} \lesssim$ 97 GeV unexcluded. However, since all the analyses, except for the hZ $\rightarrow \tau^+\tau^-$q$\bar{\rm q}$ channel, are optimised for the Higgs boson decays into b$\bar{\rm b}$, they do not provide sufficient sensitivity to the parameter regions where the effective couplings Hb$\bar{\rm b}$ and hb$\bar{\rm b}$ are suppressed [24]. The observed exclusion is presented in Figure 5b.

Exclusion plots in the (tanβ,$m_{\rm h}$) and (tanβ,$m_{\rm A}$) planes for the "large$-\mu$" scenario are presented in Figures 5c and 5d, respectively. Limits on Higgs boson masses are derived as:

$$m_{\rm h} > 84.5 \text{ GeV}, \qquad m_{\rm A} > 86.5 \text{ GeV}.$$

The expected values are 87.2 GeV and 89.2 GeV, respectively. Furthermore, the range $0.7 <$ tan$\beta < 6.7$ is excluded, for values of $m_{\rm A}$ up to 400 GeV. The allowed area between tan$\beta = 15$ and tan$\beta = 50$ corresponds to reduced Hb$\bar{\rm b}$ or hb$\bar{\rm b}$ couplings. The unexcluded region at $m_{\rm A}$ $\sim$ 88 GeV and tan$\beta \sim 15$ is caused by a slight upward fluctuation in the data, coming mainly from hA $\rightarrow$ b$\bar{\rm b}$b$\bar{\rm b}$ candidates selected in the data at $\sqrt{\rm s} > 203$ GeV. The allowed vertical narrow band at $m_{\rm A} = 107-110$ GeV and tan$\beta \gtrsim 10$ represents the region where the hA production is kinematically inaccessible and $\cos^2(\beta-\alpha) \approx \sin^2(\beta-\alpha) \approx 0.5$ so that both the hZ and HZ production cross sections are reduced by a factor of 2 with respect to $\sigma^{\rm SM}_{\rm HZ}$. Although the L3 combined search has a sensitivity for exclusion of this critical region, as can be seen from Figure 5a, the expected median confidence level is only slightly lower than 5% and an insignificant upward fluctuation observed in the data pushes the observed confidence level, $\rm CL_s$, above 5%, thus not allowing to exclude this region at 95% confidence level. Finally, the allowed area at tanβ between 6.7 and 10 and $m_{\rm h}$ between 90 and 100 GeV arises due to the excesses already discussed.

In conclusion, no evidence for neutral Higgs bosons of the MSSM is found and large regions of its parameter space are excluded.

[2)] The hZ $\rightarrow$ AAq$\bar{\rm q}$ analysis is used instead of the four-jet one whenever it provides better sensitivity, *i.e.* gives smaller values of $\rm CL_{med}$.

References

[1] H. P. Nilles, Phys. Rep. **110** (1984) 1;H. E. Haber and G. L. Kane, Phys. Rep. **117** (1985) 75;R. Barbieri, Riv. Nuovo Cim. **11 n°4** (1988) 1

[2] J.F. Gunion *et al.*, in The Higgs Hunter's Guide, (Addison Wesley, 1990), p. 191

[3] D.E. Groom *et al.*, Eur. Phys. J. **C 15** (2000) 1

[4] L3 Collaboration, M. Acciarri *et al.*, Phys. Lett. **B 503** (2001) 21

[5] L3 Collaboration, M. Acciarri *et al.*, Phys. Lett. **B 471** (1999) 321

[6] OPAL Collaboration, G. Abbiendi *et al.*, Eur. Phys. J. **C 12** (2000) 567;ALEPH Collaboration, A. Heister *et al.*, Phys. Lett. **B 526** (2002) 191;DELPHI Collaboration, J. Abdallah *et al.*, Eur. Phys. J. **C 23** (2002) 409

[7] L3 Collab., B. Adeva *et al.*, Nucl. Instr. Meth. **A 289** (1990) 35;
J.A. Bakken *et al.*, Nucl. Instr. Meth. **A 275** (1989) 81;
O. Adriani *et al.*, Nucl. Instr. Meth. **A 302** (1991) 53;
B. Adeva *et al.*, Nucl. Instr. Meth. **A 323** (1992) 109;
K. Deiters *et al.*, Nucl. Instr. Meth. **A 323** (1992) 162;
M. Chemarin *et al.*, Nucl. Instr. Meth. **A 349** (1994) 345;
M. Acciarri *et al.*, Nucl. Instr. Meth. **A 351** (1994) 300;
G. Basti *et al.*, Nucl. Instr. Meth. **A 374** (1996) 293;
A. Adam *et al.*, Nucl. Instr. Meth. **A 383** (1996) 342

[8] M. Carena *et al.*, Preprint CERN-TH/99-374

[9] S.Heinemeyer, W.Hollik, G. Weiglein, Eur. Phys. J. **C9** (1999) 343;S. Heinemeyer, W. Hollik, G. Weiglein, Phys. Rev. **D 58** (1998) 091701;S. Heinemeyer, W. Hollik, G. Weiglein, Phys. Lett. **B 440** (1998) 296

[10] M. Carena, M. Quiros and C. E. M. Wagner, Nucl. Phys. **B 461** (1996) 407;H. Haber, R. Hempfling, A. Hoang, Z. Phys. **C 75** (1997) 539

[11] P. Janot, "The HZHA generator", in "Physics at LEP2", CERN Report 96-01 (1996), Version 3, released in December 1999,
`http://alephwww.cern.ch/~janot/Generators.html`

[12] PYTHIA versions 5.722 and 6.1 are used.
T. Sjöstrand, Preprint CERN-TH/7112/93 (1993), revised August 1995; Comp. Phys. Comm. **82** (1994) 74; Preprint hep-ph/0001032 (2000)

[13] KK2f version 4.13 is used;
S. Jadach, B.F.L. Ward and Z. Wąs, Comp. Phys. Comm. **130** (2000) 260

[14] KORALW version 1.33 is used.
S. Jadach *et al.*, Comp. Phys. Comm. **94** (1996) 216;
S. Jadach *et al.*, Phys. Lett. **B 372** (1996) 289

[15] KORALZ version 4.02 is used.
S. Jadach, B.F.L. Ward and Z. Wąs, Comp. Phys. Comm. **79** (1994) 503

[16] PHOJET version 1.05 is used.
R. Engel, Z. Phys. **C 66** (1995) 203;
R. Engel and J. Ranft, Phys. Rev. **D 54** (1996) 4244

[17] F. A. Berends, R. Pittau and R. Kleiss, Comp. Phys. Comm. **85** (1995) 437

[18] GEANT version 3.15 is used; R. Brun *et al.*, Preprint CERN DD/EE/84-1 (1984), revised 1987

[19] H. Fesefeldt, Report RWTH Aachen PITHA 85/02 (1985)

[20] L3 Collaboration, P. Achard *et al.*, Phys. Lett. **B 517** (2001) 319

[21] S. Bethke *et al.*, Nucl. Phys. **B 370** (1992) 310

[22] A. Read, "Modified Frequentist Analysis of Search Results" in *Workshop on Confidence Limits*, eds. F. James, L.Lyons and Y.Perrin, CERN 2000-05, p. 81

[23] R. D. Cousins and V. L. Highland, Nucl. Inst. Meth. **A 320** (1992) 331

[24] W. Loinaz and J.D. Wells, Phys. Lett. **B 445** (1998) 178;H. Baer and J.D. Wells, Phys. Rev. **D 57** (1998) 4446;M. Carena, S. Mrenna, C.E.M. Wagner, Phys. Rev. **D 60** (1999) 075010

[25] OPAL Collaboration, G. Alexander *et al.*, Z. Phys. **C 73** (1997) 189.

The L3 Collaboration:

P.Achard,[21] O.Adriani,[18] M.Aguilar-Benitez,[25] J.Alcaraz,[25,19] G.Alemanni,[23] J.Allaby,[19] A.Aloisio,[29] M.G.Alviggi,[29] H.Anderhub,[47] V.P.Andreev,[6,34] F.Anselmo,[9] A.Arefiev,[28] T.Azemoon,[3] T.Aziz,[10,19] P.Bagnaia,[39] A.Bajo,[25] G.Baksay,[26] L.Baksay,[26] S.V.Baldew,[2] S.Banerjee,[10] Sw.Banerjee,[4] A.Barczyk,[47,45] R.Barillère,[19] P.Bartalini,[23] M.Basile,[9] N.Batalova,[44] R.Battiston,[33] A.Bay,[23] F.Becattini,[18] U.Becker,[14] F.Behner,[47] L.Bellucci,[18] R.Berbeco,[3] J.Berdugo,[25] P.Berges,[14] B.Bertucci,[33] B.L.Betev,[47] M.Biasini,[33] M.Biglietti,[29] A.Biland,[47] J.J.Blaising,[4] S.C.Blyth,[35] G.J.Bobbink,[2] A.Böhm,[1] L.Boldizsar,[13] B.Borgia,[39] S.Bottai,[18] D.Bourilkov,[47] M.Bourquin,[21] S.Braccini,[21] J.G.Branson,[41] F.Brochu,[4] J.D.Burger,[14] W.J.Burger,[33] X.D.Cai,[14] M.Capell,[14] G.Cara Romeo,[9] G.Carlino,[29] A.Cartacci,[18] J.Casaus,[25] F.Cavallari,[39] N.Cavallo,[36] C.Cecchi,[33] M.Cerrada,[25] M.Chamizo,[21] Y.H.Chang,[49] M.Chemarin,[24] A.Chen,[49] G.Chen,[7] G.M.Chen,[7] H.F.Chen,[22] H.S.Chen,[7] G.Chiefari,[29] L.Cifarelli,[40] F.Cindolo,[9] I.Clare,[14] R.Clare,[38] G.Coignet,[4] N.Colino,[25] S.Costantini,[39] B.de la Cruz,[25] S.Cucciarelli,[33] J.A.van Dalen,[31] R.de Asmundis,[29] P.Déglon,[21] J.Debreczeni,[13] A.Degré,[4] K.Dehmelt,[26] K.Deiters,[45] D.della Volpe,[29] E.Delmeire,[21] P.Denes,[37] F.DeNotaristefani,[39] A.De Salvo,[47] M.Diemoz,[39] M.Dierckxsens,[2] C.Dionisi,[39] M.Dittmar,[47,19] A.Doria,[29] M.T.Dova,[11,♯] D.Duchesneau,[4] B.Echenard,[21] A.Eline,[19] H.El Mamouni,[24] A.Engler,[35] F.J.Eppling,[14] A.Ewers,[1] P.Extermann,[21] M.A.Falagan,[25] S.Falciano,[39] A.Favara,[32] J.Fay,[24] O.Fedin,[34] M.Felcini,[47] T.Ferguson,[35] H.Fesefeldt,[1] E.Fiandrini,[33] J.H.Field,[21] F.Filthaut,[31] P.H.Fisher,[14] W.Fisher,[37] I.Fisk,[41] G.Forconi,[14] K.Freudenreich,[47] C.Furetta,[27] Yu.Galaktionov,[28,14] S.N.Ganguli,[10] P.Garcia-Abia,[5,19] M.Gataullin,[32] S.Gentile,[39] S.Giagu,[39] Z.F.Gong,[22] G.Grenier,[24] O.Grimm,[47] M.W.Gruenewald,[17] M.Guida,[40] R.van Gulik,[2] V.K.Gupta,[37] A.Gurtu,[10] L.J.Gutay,[44] D.Haas,[5] R.Sh.Hakobyan,[31] D.Hatzifotiadou,[9] T.Hebbeker,[1] A.Hervé,[19] J.Hirschfelder,[35] H.Hofer,[47] M.Hohlmann,[26] G.Holzner,[47] S.R.Hou,[49] Y.Hu,[31] B.N.Jin,[7] L.W.Jones,[3] P.de Jong,[2] I.Josa-Mutuberría,[25] D.Käfer,[1] M.Kaur,[15] M.N.Kienzle-Focacci,[21] J.K.Kim,[43] J.Kirkby,[19] W.Kittel,[31] A.Klimentov,[14,28] A.C.König,[31] M.Kopal,[44] V.Koutsenko,[14,28] M.Kräber,[47] R.W.Kraemer,[35] W.Krenz,[1] A.Krüger,[46] A.Kunin,[14] P.Ladron de Guevara,[25] I.Laktineh,[24] G.Landi,[18] M.Lebeau,[19] A.Lebedev,[14] P.Lebrun,[24] P.Lecomte,[47] P.Lecoq,[19] P.Le Coultre,[47] J.M.Le Goff,[19] R.Leiste,[46] M.Levtchenko,[27] P.Levtchenko,[34] C.Li,[22] S.Likhoded,[46] C.H.Lin,[49] W.T.Lin,[49] F.L.Linde,[2] L.Lista,[29] Z.A.Liu,[7] W.Lohmann,[46] E.Longo,[39] Y.S.Lu,[7] K.Lübelsmeyer,[1] C.Luci,[39] L.Luminari,[39] W.Lustermann,[47] W.G.Ma,[22] L.Malgeri,[21] A.Malinin,[28] C.Maña,[25] D.Mangeol,[31] J.Mans,[37] J.P.Martin,[24] F.Marzano,[39] K.Mazumdar,[10] R.R.McNeil,[6] S.Mele,[19,29] L.Merola,[29] M.Meschini,[18] W.J.Metzger,[31] A.Mihul,[12] H.Milcent,[19] G.Mirabelli,[39] J.Mnich,[1] G.B.Mohanty,[10] G.S.Muanza,[24] A.J.M.Muijs,[2] B.Musicar,[41] M.Musy,[39] S.Nagy,[16] S.Natale,[21] M.Napolitano,[29] F.Nessi-Tedaldi,[47] H.Newman,[32] T.Niessen,[1] A.Nisati,[39] H.Nowak,[46] R.Ofierzynski,[47] G.Organtini,[39] C.Palomares,[19] D.Pandoulas,[1] P.Paolucci,[29] R.Paramatti,[39] G.Passaleva,[18] S.Patricelli,[29] T.Paul,[11] M.Pauluzzi,[33] C.Paus,[14] F.Pauss,[47] M.Pedace,[39] S.Pensotti,[27] D.Perret-Gallix,[4] B.Petersen,[31] D.Piccolo,[29] F.Pierella,[9] M.Pioppi,[33] P.A.Piroué,[37] E.Pistolesi,[27] V.Plyaskin,[28] M.Pohl,[21] V.Pojidaev,[18] J.Pothier,[19] D.O.Prokofiev,[44] D.Prokofiev,[34] J.Quartieri,[40] G.Rahal-Callot,[47] M.A.Rahaman,[10] P.Raics,[16] N.Raja,[10] R.Ramelli,[47] P.G.Rancoita,[27] R.Ranieri,[18] A.Raspereza,[46] P.Razis,[30] D.Ren,[47] M.Rescigno,[39] S.Reucroft,[11] S.Riemann,[46] K.Riles,[3] B.P.Roe,[3] L.Romero,[25] A.Rosca,[8] S.Rosier-Lees,[4] S.Roth,[1] C.Rosenbleck,[1] B.Roux,[31] J.A.Rubio,[19] G.Ruggiero,[18] H.Rykaczewski,[47] A.Sakharov,[47] S.Saremi,[6] S.Sarkar,[39] J.Salicio,[19] E.Sanchez,[25] M.P.Sanders,[31] C.Schäfer,[19] V.Schegelsky,[34] S.Schmidt-Kaerst,[1] D.Schmitz,[1] H.Schopper,[48] D.J.Schotanus,[31] G.Schwering,[1] C.Sciacca,[29] L.Servoli,[33] S.Shevchenko,[32] N.Shivarov,[42] V.Shoutko,[14] E.Shumilov,[28] A.Shvorob,[32] T.Siedenburg,[1] D.Son,[43] C.Souga,[24] P.Spillantini,[18] M.Steuer,[14] D.P.Stickland,[37] B.Stoyanov,[42] A.Straessner,[19] K.Sudhakar,[10] G.Sultanov,[42] L.Z.Sun,[22] S.Sushkov,[8] H.Suter,[47] J.D.Swain,[11] Z.Szillasi,[26,¶] X.W.Tang,[7] P.Tarjan,[16] L.Tauscher,[5] L.Taylor,[11] B.Tellili,[24] D.Teyssier,[24] C.Timmermans,[31] Samuel C.C.Ting,[14] S.M.Ting,[14] S.C.Tonwar,[10,19] J.Tóth,[13] C.Tully,[37] K.L.Tung,[7] J.Ulbricht,[47] E.Valente,[39] R.T.Van de Walle,[31] R.Vasquez,[44] V.Veszpremi,[26] G.Vesztergombi,[13] I.Vetlitsky,[28] D.Vicinanza,[40] G.Viertel,[47] S.Villa,[38] M.Vivargent,[4] S.Vlachos,[5] I.Vodopianov,[34] H.Vogel,[35] H.Vogt,[46] I.Vorobiev,[35,28] A.A.Vorobyov,[34] M.Wadhwa,[5] W.Wallraff,[1] X.L.Wang,[22] Z.M.Wang,[22] M.Weber,[1] P.Wienemann,[1] H.Wilkens,[31] S.Wynhoff,[37] L.Xia,[32] Z.Z.Xu,[22] J.Yamamoto,[3] B.Z.Yang,[22] C.G.Yang,[7] H.J.Yang,[3] M.Yang,[7] S.C.Yeh,[50] An.Zalite,[34] Yu.Zalite,[34] Z.P.Zhang,[22] J.Zhao,[22] G.Y.Zhu,[7] R.Y.Zhu,[32] H.L.Zhuang,[7] A.Zichichi,[9,19,20] B.Zimmermann,[47] M.Zöller.[1]

1 I. Physikalisches Institut, RWTH, D-52056 Aachen, Germany[§]
III. Physikalisches Institut, RWTH, D-52056 Aachen, Germany[§]
2 National Institute for High Energy Physics, NIKHEF, and University of Amsterdam, NL-1009 DB Amsterdam, The Netherlands
3 University of Michigan, Ann Arbor, MI 48109, USA
4 Laboratoire d'Annecy-le-Vieux de Physique des Particules, LAPP,IN2P3-CNRS, BP 110, F-74941 Annecy-le-Vieux CEDEX, France
5 Institute of Physics, University of Basel, CH-4056 Basel, Switzerland
6 Louisiana State University, Baton Rouge, LA 70803, USA
7 Institute of High Energy Physics, IHEP, 100039 Beijing, China[△]
8 Humboldt University, D-10099 Berlin, Germany[§]
9 University of Bologna and INFN-Sezione di Bologna, I-40126 Bologna, Italy
10 Tata Institute of Fundamental Research, Mumbai (Bombay) 400 005, India
11 Northeastern University, Boston, MA 02115, USA
12 Institute of Atomic Physics and University of Bucharest, R-76900 Bucharest, Romania
13 Central Research Institute for Physics of the Hungarian Academy of Sciences, H-1525 Budapest 114, Hungary[‡]
14 Massachusetts Institute of Technology, Cambridge, MA 02139, USA
15 Panjab University, Chandigarh 160 014, India.
16 KLTE-ATOMKI, H-4010 Debrecen, Hungary[¶]
17 Department of Experimental Physics, University College Dublin, Belfield, Dublin 4, Ireland
18 INFN Sezione di Firenze and University of Florence, I-50125 Florence, Italy
19 European Laboratory for Particle Physics, CERN, CH-1211 Geneva 23, Switzerland
20 World Laboratory, FBLJA Project, CH-1211 Geneva 23, Switzerland
21 University of Geneva, CH-1211 Geneva 4, Switzerland
22 Chinese University of Science and Technology, USTC, Hefei, Anhui 230 029, China[△]
23 University of Lausanne, CH-1015 Lausanne, Switzerland
24 Institut de Physique Nucléaire de Lyon, IN2P3-CNRS,Université Claude Bernard, F-69622 Villeurbanne, France
25 Centro de Investigaciones Energéticas, Medioambientales y Tecnológicas, CIEMAT, E-28040 Madrid, Spain[♭]
26 Florida Institute of Technology, Melbourne, FL 32901, USA
27 INFN-Sezione di Milano, I-20133 Milan, Italy
28 Institute of Theoretical and Experimental Physics, ITEP, Moscow, Russia
29 INFN-Sezione di Napoli and University of Naples, I-80125 Naples, Italy
30 Department of Physics, University of Cyprus, Nicosia, Cyprus
31 University of Nijmegen and NIKHEF, NL-6525 ED Nijmegen, The Netherlands
32 California Institute of Technology, Pasadena, CA 91125, USA
33 INFN-Sezione di Perugia and Università Degli Studi di Perugia, I-06100 Perugia, Italy
34 Nuclear Physics Institute, St. Petersburg, Russia
35 Carnegie Mellon University, Pittsburgh, PA 15213, USA
36 INFN-Sezione di Napoli and University of Potenza, I-85100 Potenza, Italy
37 Princeton University, Princeton, NJ 08544, USA
38 University of Californa, Riverside, CA 92521, USA
39 INFN-Sezione di Roma and University of Rome, "La Sapienza", I-00185 Rome, Italy
40 University and INFN, Salerno, I-84100 Salerno, Italy
41 University of California, San Diego, CA 92093, USA
42 Bulgarian Academy of Sciences, Central Lab. of Mechatronics and Instrumentation, BU-1113 Sofia, Bulgaria
43 The Center for High Energy Physics, Kyungpook National University, 702-701 Taegu, Republic of Korea
44 Purdue University, West Lafayette, IN 47907, USA
45 Paul Scherrer Institut, PSI, CH-5232 Villigen, Switzerland
46 DESY, D-15738 Zeuthen, Germany
47 Eidgenössische Technische Hochschule, ETH Zürich, CH-8093 Zürich, Switzerland
48 University of Hamburg, D-22761 Hamburg, Germany
49 National Central University, Chung-Li, Taiwan, China
50 Department of Physics, National Tsing Hua University, Taiwan, China
§ Supported by the German Bundesministerium für Bildung, Wissenschaft, Forschung und Technologie
‡ Supported by the Hungarian OTKA fund under contract numbers T019181, F023259 and T037350.
¶ Also supported by the Hungarian OTKA fund under contract number T026178.
♭ Supported also by the Comisión Interministerial de Ciencia y Tecnología.
♯ Also supported by CONICET and Universidad Nacional de La Plata, CC 67, 1900 La Plata, Argentina.
△ Supported by the National Natural Science Foundation of China.

Scenario	M_{SUSY} [GeV]	M_2 [GeV]	μ [GeV]	X_t [GeV]	M_3 [GeV]
"m_h−max"	1000	200	−200	$2M_{SUSY}$	800
"no mixing"	1000	200	−200	0	800
"large−μ"	400	400	1000	−300	200

Table 1: Values of the MSSM parameters for the three scenarios considered in this Letter.

"m_h−max" scenario			
(m_A,m_h) [GeV]	(90,90)		(165,110)
tanβ	25		3
Preselection			
Data	2096		
Background	2044		
$\epsilon(hA \to b\bar{b}b\bar{b})$	94%		–
$\epsilon(hZ \to b\bar{b}q\bar{q})$	89%		92%
hA signal	7.2		–
hZ signal	0.66		18.4
Selection			
Analysis branch	hA	hZ	hZ
Data	25	275	121
Background	28.9	259	120
$\epsilon(hA \to b\bar{b}b\bar{b})$	56%	19%	–
$\epsilon(hZ \to b\bar{b}q\bar{q})$	25%	37%	63%
hA signal	4.3	1.5	–
hZ signal	0.18	0.28	12.6
$s/b > 0.05$			
Data	18		42
Background	21.3		42.1
$\epsilon(hA \to b\bar{b}b\bar{b})$	56%		–
$\epsilon(hZ \to b\bar{b}q\bar{q})$	28%		55%
hA signal	4.3		–
hZ signal	0.21		11.0

Table 2: The number of data, expected background, expected signal events and signal efficiencies in the four-jet channel after preselection, after final selection and after applying a cut on the final discriminants corresponding to a signal-to-background ratio greater than 0.05. This cut is used to calculate the confidence levels. Numbers are given for two Higgs mass hypotheses in the "m_h−max" scenario.

"$m_{\mathrm{h}}-$max" scenario		
$(m_{\mathrm{A}},m_{\mathrm{h}})$ [GeV]	(90,90)	(165,110)
$\tan\beta$	25	3
Selection		
Data	28	8
Background	27.4	6.4
$\epsilon(\mathrm{hA} \to \mathrm{b\bar{b}}\tau^+\tau^-)$	41%	–
$\epsilon(\mathrm{hA} \to \tau^+\tau^-\mathrm{b\bar{b}})$	41%	–
$\epsilon(\mathrm{hZ} \to \mathrm{b\bar{b}}\tau^+\tau^-)$	22%	33%
$\epsilon(\mathrm{hZ} \to \tau^+\tau^-\mathrm{q\bar{q}})$	21%	32%
hA signal	0.50	–
hZ signal	0.03	0.78
$s/b > 0.05$		
Data	2	3
Background	1.6	2.8
$\epsilon(\mathrm{hA} \to \mathrm{b\bar{b}}\tau^+\tau^-)$	34%	–
$\epsilon(\mathrm{hA} \to \tau^+\tau^-\mathrm{b\bar{b}})$	30%	–
$\epsilon(\mathrm{hZ} \to \mathrm{b\bar{b}}\tau^+\tau^-)$	19%	30%
$\epsilon(\mathrm{hZ} \to \tau^+\tau^-\mathrm{q\bar{q}})$	14%	29%
hA signal	0.39	–
hZ signal	0.02	0.70

Table 3: The number of data, expected background, expected signal events and signal efficiencies in the channels containing tau leptons after selection and after applying a cut on the final discriminants corresponding to a signal-to-background ratio greater than 0.05. This cut is used to calculate the confidence levels. Numbers are given for two Higgs mass hypotheses in the "$m_{\mathrm{h}}-$max" scenario.

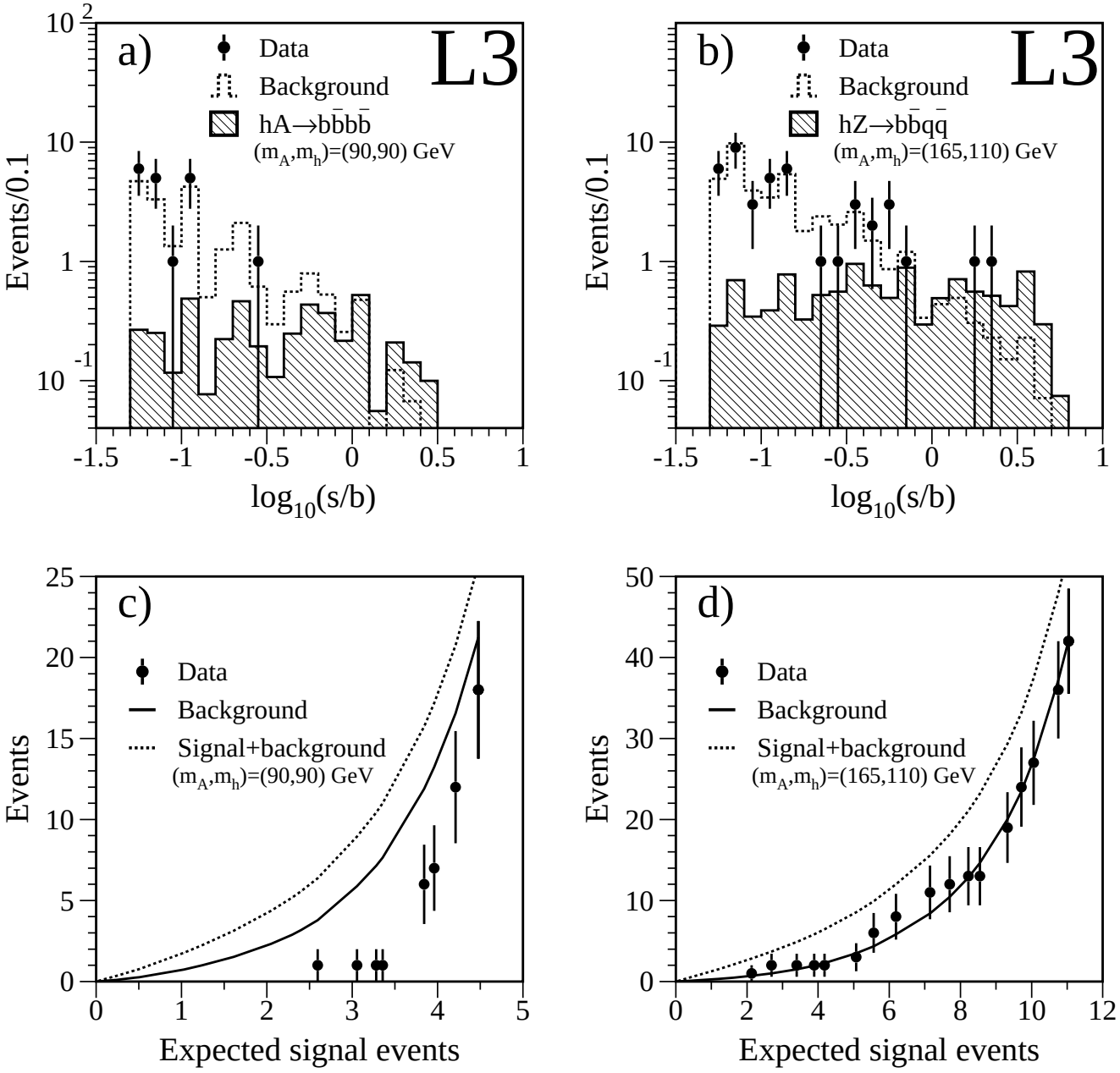

Figure 1: The distribution of data, expected background and expected signal events as a function of the logarithm of the signal-to-background ratio, $\log_{10}$(s/b), in the four-jet channel for the Higgs boson mass hypotheses a) ($m_{\rm A}$,$m_{\rm h}$) = (90,90) GeV and b) ($m_{\rm A}$,$m_{\rm h}$) = (165,110) GeV. Integrated distributions of data and expected background events as a function of the expected signal are shown in c) and d).

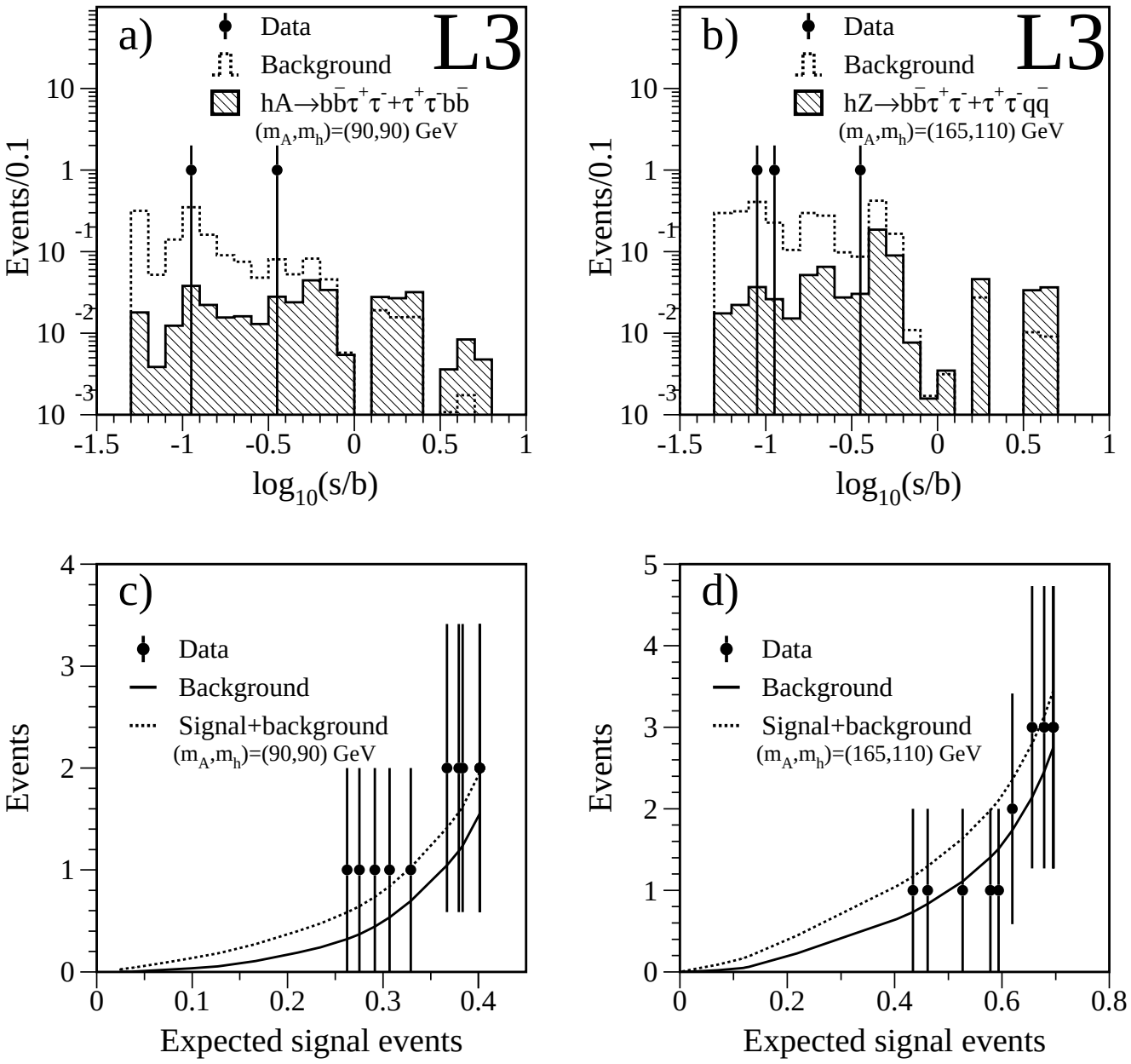

Figure 2: The distribution of data, expected background and expected signal events as a function of the logarithm of the signal-to-background ratio, $\log_{10}$(s/b), in the channels containing tau leptons for the Higgs boson mass hypotheses a) (m_{A},m_{h}) = (90,90) GeV and b) (m_{A},m_{h}) = (165,110) GeV. Integrated distributions of data and expected background events as a function of the expected signal are shown in c) and d).

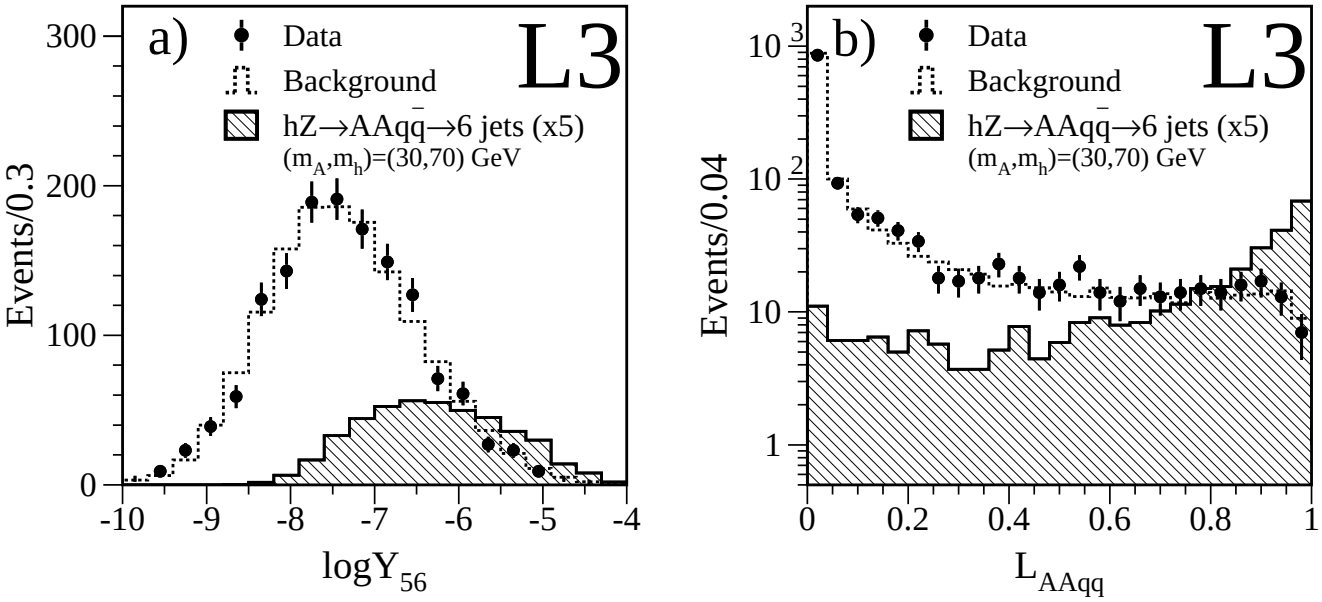

Figure 3: Distributions of a) $\log Y_{56}$ and b) L_{AAqq} in the $hZ \to AA q\bar{q} \to q\bar{q}q'\bar{q}'q''\bar{q}''$ channel. The points are data collected at $\sqrt{s} = 203-209$ GeV, the dashed lines are the expected background and the hatched histograms are the signal corresponding to the Higgs boson mass hypothesis $(m_A,m_h) = (30,70)$ GeV. The signal expectation is calculated within the "no mixing" scenario at $\tan\beta = 0.75$ and is multiplied by a factor of 5.

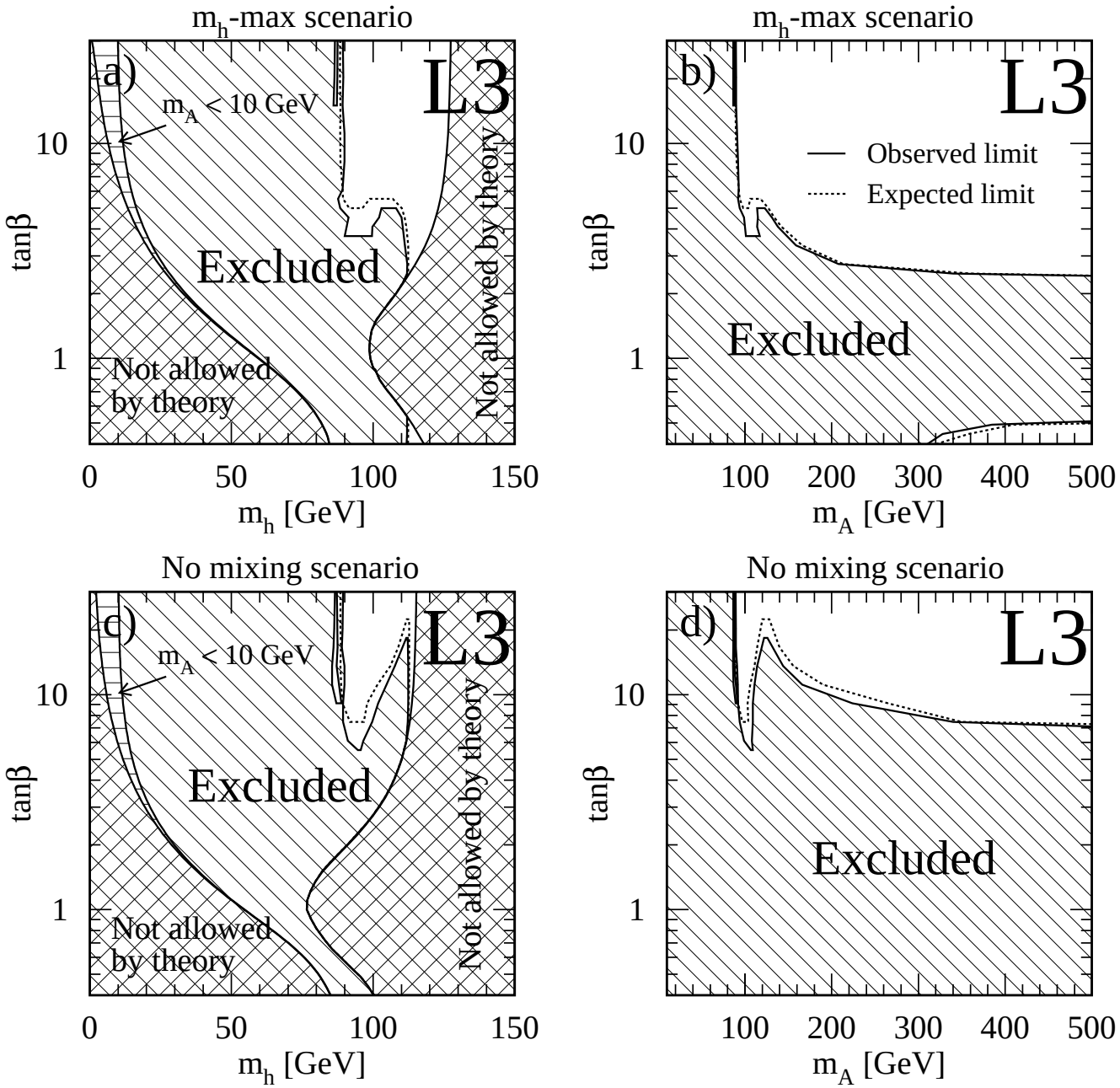

Figure 4: Exclusion contours in the (tanβ,$m_{\rm h}$) and (tanβ,$m_{\rm A}$) planes at 95% confidence level for the "$m_{\rm h}-$max" and "no mixing" scenarios. The hatched area represents the exclusion and the crossed area is not allowed by theory. The horizontally hatched area corresponds to $m_{\rm A} < 10$ GeV and was previously excluded by LEP [25]. The dashed line indicates the expected exclusion in the absence of a signal.

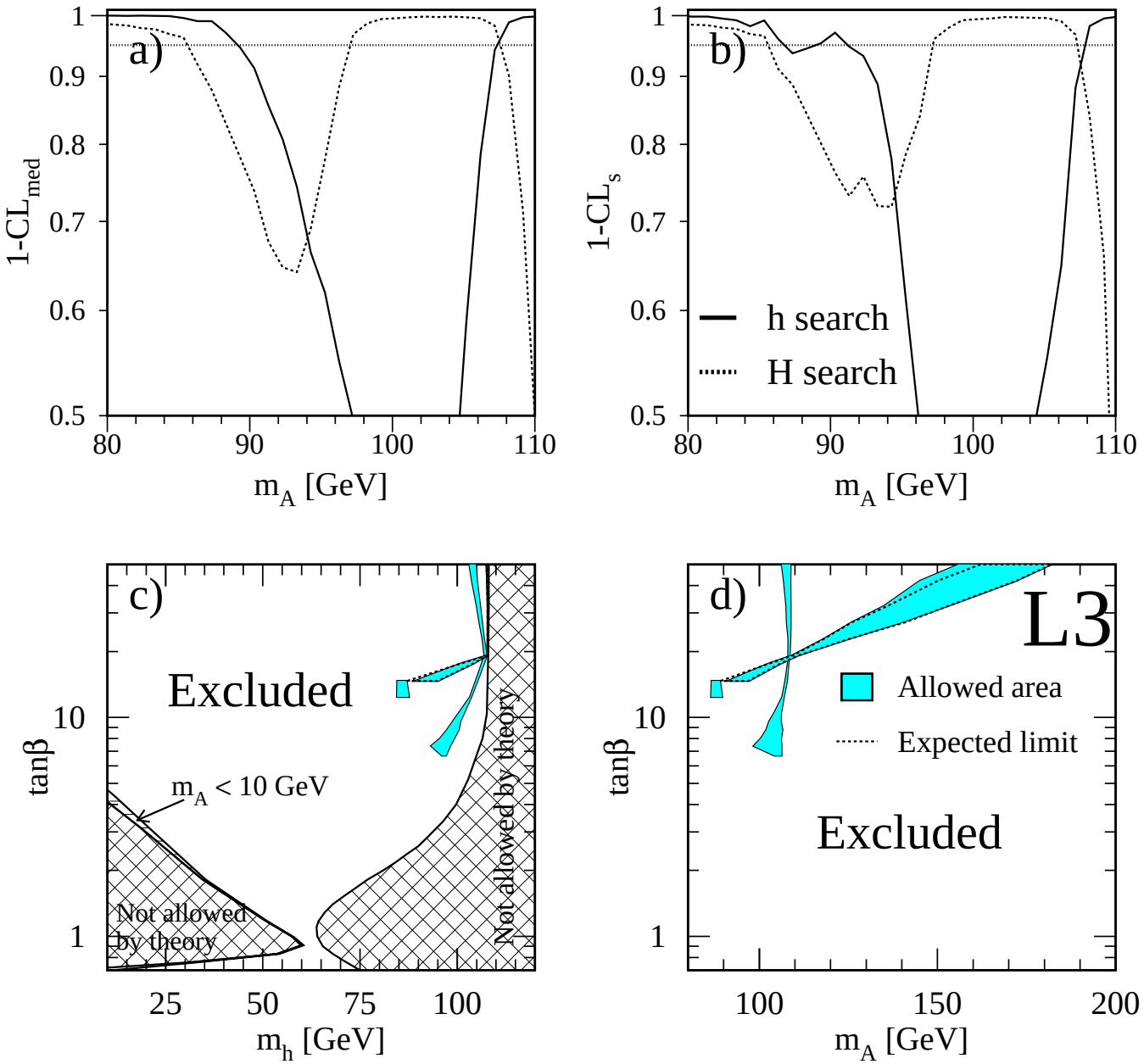

Figure 5: Confidence levels a) $(1-\mathrm{CL_{med}})$ and b) $(1-\mathrm{CL_s})$ as a function of m_A at $\tan\beta = 15$ obtained for the h boson (solid line), and the H boson (dashed line) searches in the "large$-\mu$" scenario. Exclusion contours in the c) $(\tan\beta, m_\mathrm{h})$ and d) $(\tan\beta, m_\mathrm{A})$ planes for the "large$-\mu$" scenario. The crossed area is theoretically inaccessible, the open area is excluded at 95% confidence level and the shaded area is experimentally allowed. The dashed line represents the expected boundary of the allowed region in the absence of a signal.